Numerical Simulation of a Nonequilibrium Plasma Flow in a Nitrogen Arcjet Thruster Using a Three-Temperature Kinetic Model

Shigeru KUCHI-ISHI* and Michio NISHIDA**
Department of Aeronautics and Astronautics, Kyushu University
Fukuoka 812-81, Japan

Abstract

A plasma flow within a DC arcjet thruster has been modeled and analyzed numerically. Nitrogen is employed as a working gas. Not only chemical but also thermal nonequilibrium effects are considered here, namely heavy particle translational, vibrational and electron translational temperatures are separately treated. In the present paper, the governing equations of the flow field and the electric field, accompanying chemical models and numerical methods are presented. A preliminary calculation with total current of 1 A has also been conducted and results and remaining problems are discussed.

Nomenclature

D	=	diffusion coefficient
E	=	energy per unit volume
$E_{\rm D}$	=	dissociation energy per unit mass
$E_{\rm I}$	=	ionization energy per unit mass
$\widetilde{E}$	=	electric field
e	=	energy per unit mass, charge of electron
h	=	static enthalpy per unit mass
Δh^0	=	heat of formation at absolute zero
j	=	electric current density
j_i	=	cuurent density tensor, $i = 1 \sim 3$
k	=	Boltzmann constant
m	=	particle mass
n	=	number density
p	=	static pressure
Q	=	energy transfer rate
R	=	gas constant
T	=	translational temperature
t	=	time
u_i	=	velocity tensor, $i = 1 \sim 3$
V	=	arc voltage
X	=	mole fraction
x_i	=	coordinate tensor, $i = 1 \sim 3$
$\dot{w}$	=	mass production rate
ν	=	collision frequency
$\widetilde{\sigma}$	=	electrical conductivity
μ	=	coefficient of viscosity
ϕ	=	electric potential
ρ	=	mass density
$\theta_{\rm vib}$	=	characteristic temperature of vibration
λ	=	coefficient of thermal conductivity

Subscripts and superscripts

e	=	electron
eq	=	equilibrium
M	=	molecular species
ns	=	number of species, ns = 5
rot	=	rotational mode
s	=	species index
tr	=	translational mode
vib	=	vibrational mode

*Graduate Student

**Professor

1. Introduction

Arcjet thrusters have attracted much interest as one of the available propulsion systems for north-south station keeping of future spacecrafts. In order to predict the performance characteristics of the arcjet thruster, it is necessary to investigate the detail of the flow field interacting with arc currents inside the thruster. However, it is actually difficult to directly observe the discharge section. Therefore, we have applied a computational technique to simulate the thruster flow field. The computational simulation has an advantage of easily varying parameters such as thruster geometry, arc currents and other conditions.

With the development of computational environment, considerably many computational studies of arcjet thrusters and related modeling have been extensively conducted. Reference 1 may be cited as a recent review describing the physical modeling of the arcjet and up to date numerical simulations of arcjet thruster flows. Pioneering computations are those of Refs. 2 and 3, where partially ionized one-temperature argon was treated as propellant but nonequilibrium ionization kinetics was included into the modeling. These two were, thereafter, extended to the Navier-Stokes analysis to simulate a practical radiation-cooled arcjet thruster,[4-6] but monatomic

gas (argon) and a one-temperature model were still employed. In practical arcjet thrusters, electron gas gains energy through Joule heating and then electron energy is transferred to heavy-particles due to elastic and inelastic collisions, resulting in an increase in translational temperature (and vibrational temperature for molecular species) of heavy particles. This process is considered as out of equilibrium, and hence a two-temperature model is appropriate to the arcjet modeling. References 7 to 9 are cited as the typical studies of numerical simulation using a thermal nonequilibrium model consisting of heavy-particle translational temperature and electron temperature.

A more detailed modeling of thermal nonequilibrium for molecular gas will be a three-temperature model, consisting of heavy particle translational temperature, vibrational temperature and electron temperature. In this case, not only translational energy but also vibrational and dissociation energies are necessary to be converted to directed kinetic energy through an expansion in the thruster nozzle. However, thermochemical equilibrium does not exist in the expanding flow, so that vibrational energy and dissociation energy are not likely to contribute to the thrust. Therefore, it is the aim of the present study to investigate thermal nonequilibrium effects in the expansion of high-temperature propellant gas, thereby it can be clarified how much vibrational and dissociation energies are converted to thrust.

2. Flow Model

In the present study, numerical simulations of a flow in a small power arcjet thruster with nitrogen as propellant have been performed for the same nozzle geometry as used in laboratory experiments (Fig. 1). A flow model introduced here is based on a flow

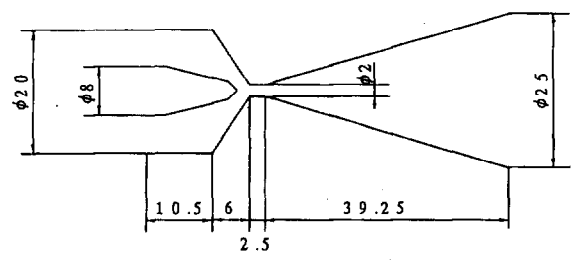

Figure 1. Thruster geometry (unit: mm)

situation realized in an actual arcjet thruster. With assuming chemical and thermal nonequilibrium flow discussed in the previous section, it is composed of:

1. the flow is axisymmetric and viscous,
2. nitrogen is considered as propellant,
3. vibrational excitations are populated by Boltzmann equilibrium,
4. rotational temperature of molecules are fully equilibrated with translational temperature of heavy species,
5. species considered are N_2, N, N_2^+, N^+, e^-,
6. equal velocity is considered for all heavy particles,
7. an inflow to the thruster is subsonic and the flow at the nozzle exit is supersonic,
8. Lorentz force is neglected due to very weak magnetic field induced by small arc currents.

3. Basic Equations

3.1 Fluid dynamic equations

Propellant flow equations are the Navier-Stokes equations extended to chemical and thermal nonequilibrium gases, which can be expressed in unsteady form as

Total mass conservation:

$$\frac{\partial \rho}{\partial t} + \frac{\partial (\rho u_j)}{\partial x_j} = 0 \tag{1}$$

Momentum conservation for each directions:

$$\frac{\partial (\rho u_i)}{\partial t} + \frac{\partial (\rho u_i u_j + \delta_{ij} p)}{\partial x_j} = \frac{\partial}{\partial x_j}\left[\mu\left(\frac{\partial u_i}{\partial x_j} + \frac{\partial u_j}{\partial x_i}\right) - \frac{2}{3}\mu \frac{\partial u_k}{\partial x_k}\delta_{ij}\right] \tag{2}$$

Total energy conservation:

$$\begin{aligned}\frac{\partial E}{\partial t} + \frac{\partial}{\partial x_j}[(E+p)u_j] &= \frac{\partial}{\partial x_j}\left(\lambda \frac{\partial T}{\partial x_j} + \lambda_{\mathrm{vib}} \frac{\partial T_{\mathrm{vib}}}{\partial x_j} + \lambda_e \frac{\partial T_e}{\partial x_j}\right) \\ &+ \frac{\partial}{\partial x_j}\left(\rho \sum_{s=1}^{ns} h_s D_s \frac{\partial X_s}{\partial x_j}\right) \\ &+ \frac{\partial}{\partial x_j}\left[u_i \mu\left(\frac{\partial u_i}{\partial x_j} + \frac{\partial u_j}{\partial x_i}\right) - \frac{2}{3} u_i \mu \frac{\partial u_k}{\partial x_k}\delta_{ij}\right] \\ &+ j_j \widetilde{E}_j \end{aligned} \tag{3}$$

Mass conservation for each species:

$$\frac{\partial \rho_s}{\partial t} + \frac{\partial (\rho_s u_j)}{\partial x_j} = \frac{\partial}{\partial x_j}\left(\rho D_s \frac{\partial X_s}{\partial x_j}\right) + \dot{w}_s \quad (4)$$

Vibrational energy conservation:

$$\begin{aligned} &\frac{\partial E_{\rm vib}}{\partial t} + \frac{\partial (E_{\rm vib} u_j)}{\partial x_j} \\ &= \frac{\partial}{\partial x_j}\left(\lambda_{\rm vib}\frac{\partial T_{\rm vib}}{\partial x_j}\right) \\ &\quad + \frac{\partial}{\partial x_j}\left(\rho \sum_{s=\rm M} e_{{\rm vib},s} D_s \frac{\partial X_s}{\partial x_j}\right) \\ &\quad + Q_{\rm T-V} + Q_{\rm e-V} + Q_{\rm D} \end{aligned} \quad (5)$$

Electron energy conservation:

$$\begin{aligned} &\frac{\partial E_{\rm e}}{\partial t} + \frac{\partial}{\partial x_j}[(E_{\rm e} + p_{\rm e})u_j] \\ &= \frac{\partial}{\partial x_j}\left(\lambda_{\rm e}\frac{\partial T_{\rm e}}{\partial x_j}\right) + \frac{\partial}{\partial x_j}\left(\rho h_{\rm e} D_{\rm e}\frac{\partial X_{\rm e}}{\partial x_j}\right) \\ &\quad + Q_{\rm T-e} - Q_{\rm e-V} + Q_{\rm D}^{\rm e} + Q_{\rm I}^{\rm e} \\ &\quad + u_j \frac{\partial p_{\rm e}}{\partial x_j} + j_j \widetilde{E}_j \end{aligned} \quad (6)$$

Equation of state:

$$p = \sum_{s\neq \rm e} \rho_s R_s T + \rho_{\rm e} R_{\rm e} T_{\rm e} \quad (7)$$

where δ_{ij} is the Kronecker delta and each internal energies can be defined as follows:

$$\begin{aligned} E &= E_{\rm tr} + E_{\rm rot} + E_{\rm vib} + E_{\rm e} \\ &\quad + \sum_{s=1}^{\rm ns} \rho_s \Delta h_s^0 + \frac{1}{2}\rho u_j u_j \end{aligned} \quad (8)$$

$$E_{\rm tr} = \sum_{s\neq \rm e} \frac{3}{2}\rho_s R_s T \quad (9)$$

$$E_{\rm rot} = \sum_{s=\rm M} \rho_s R_s T \quad (10)$$

$$E_{\rm vib} = \sum_{s=\rm M} \frac{\rho_s R_s \theta_{{\rm vib},s}}{\exp(\theta_{{\rm vib},s}/T_{\rm vib}) - 1} \quad (11)$$

$$E_{\rm e} = \frac{3}{2}\rho_{\rm e} R_{\rm e} T_{\rm e} \quad (12)$$

The above equations are transformed to the axisymmetric coordinate system and further transformed to the generalized curvilinear coordinate system in order to apply boundary conditions easily.

3.2 Electric field equations

The arcjet thruster considered here is a low power thruster, so that discharge currents are relatively small. Hence, hall currents and ion slip may be neglected. A previous computational result[2] showed that the Lorentz force caused by the interaction of the electric current density and induced magnetic flux is very small, so that the Lorentz force term may be excluded from the present momentum equations. To evaluate the Joule heating term $j_j \widetilde{E}_j$, which appears in Eqs. (3) and (6), the electric field equations are needed that consist of the Ohm's law and Maxwell equation. They are given by

$$\boldsymbol{j} = \tilde{\sigma}\widetilde{\boldsymbol{E}} \quad (13)$$

$$\nabla \cdot \boldsymbol{j} = 0 \quad (14)$$

For the steady magnetic field, an electric field is expressed by a potential ϕ as follows:

$$\widetilde{\boldsymbol{E}} = -\nabla\phi \quad (15)$$

Eliminating $\boldsymbol{j}$ from Eqs. (13) and (14), and using the resulting equation in Eq. (15), we have

$$\nabla \cdot (\tilde{\sigma}\nabla\phi) = 0 \quad (16)$$

ϕ can be obtained by solving the above equation.

4. Nonequilibrium Model

4.1 Chemical reaction model

Chemical reactions for nitrogen considered here are given on Table 1. The rate constants for the reactions are evaluated by Park's work.[10]

Table 1 N_2-Reactions

r	Reactants		Products
1	$N_2 + N_2$	$\rightleftharpoons$	$N + N + N_2$
2	$N_2 + N$	$\rightleftharpoons$	$N + N + N$
3	$N_2 + N_2^+$	$\rightleftharpoons$	$N + N + N_2^+$
4	$N_2 + N^+$	$\rightleftharpoons$	$N + N + N^+$
5	$N_2 + e^-$	$\rightleftharpoons$	$N + N + e^-$
6	$N + N$	$\rightleftharpoons$	$N_2^+ + e^-$
7	$N_2 + N^+$	$\rightleftharpoons$	$N_2^+ + N$
8	$N + e^-$	$\rightleftharpoons$	$N^+ + e^- + e^-$

In order to account for the thermal nonequilibrium effect, the forward reaction rates for heavy particle impact dissociation reactions ($r = 1 \sim 4$) are evaluated by using "geometric average" temperature $T_{\rm a}$ proposed by Park,[10] which is defined as

$$T_{\rm a} = \sqrt{T T_{\rm vib}} \quad (17)$$

Similarly, the electron temperature is used to evaluate both forward and backward reaction rates of electron impact dissociation ($r = 5$) and ionization reaction ($r = 8$).

4.2 Energy exchange model

The energy transfers considered here are translation - vibration, translation - electron, vibration - electron and internal energy loss due to dissociation or ionization.

Translation - vibration energy exchange

The energy transfer rate per unit volume between translational and vibrational energy modes is written in the following form:

$$Q_{\mathrm{T-V}} = \sum_{s=\mathrm{M}} \rho_s \frac{e^{\mathrm{eq}}_{\mathrm{vib},s}(T) - e_{\mathrm{vib},s}(T_{\mathrm{vib}})}{\langle \tau_s \rangle} \tag{18}$$

where

$$\langle \tau_s \rangle = \langle \tau_s^{\mathrm{MW}} \rangle + \langle \tau_s^{\mathrm{P}} \rangle \tag{19}$$

$\langle \tau_s^{\mathrm{MW}} \rangle$ is the average of the vibrational relaxation times for binary mixture, which are calculated by the semi-empirical formula of Millikan & White.[11] $\langle \tau_s^{\mathrm{P}} \rangle$ is a correction term for high temperature proposed by Park.[10]

Translation - electron energy exchange

The rate of the translational energy transfer between heavy particles and electrons is given by

$$Q_{\mathrm{T-e}} = \sum_{s \neq e} n_{\mathrm{e}} \frac{2m_{\mathrm{e}}}{m_s} \nu_{\mathrm{e},s} \frac{3}{2} k(T - T_{\mathrm{e}}) \tag{20}$$

where $\nu_{\mathrm{e},s}$ is the collision frequency of electron-s species encounters. For electron-s-neutral species encounter,

$$\nu_{\mathrm{e},s} = n_s \sigma_{\mathrm{e},s} \left(\frac{8 R_{\mathrm{e}} T_{\mathrm{e}}}{\pi} \right)^{1/2} \tag{21}$$

where $\sigma_{\mathrm{e},s}$ is the cross section for electron-s species encounter, which is taken from curve fit formula of Gnoffo et al.[12] For electron-ion encounters, the effective collision frequency from the well-known Coulomb potential:

$$\nu_{\mathrm{e},s} = 3.64 \times 10^{-6} n_s \ln \Lambda / T_{\mathrm{e}}^{3/2} \tag{22}$$

is employed[13], where

$$\Lambda = 1.24 \times 10^7 \left(\frac{T_{\mathrm{e}}^3}{n_{\mathrm{e}}} \right) \tag{23}$$

In order to account for inelastic collisions, collision frequency between electron and N_2 is multiplied by a factor δ,[1,8] which is assumed to be 1000 in the present study. However, the choice of this parameter can have serious effects on the computational results obtained, as will be discussed later.

Vibration - electron energy exchange

In the present study only N_2-electron coupling is considered for vibration-electron energy exchange, which can be expressed as

$$Q_{\mathrm{e-V}} = \rho_{\mathrm{N_2}} \frac{e^{\mathrm{eq}}_{\mathrm{vib,N_2}}(T_{\mathrm{e}}) - e_{\mathrm{vib,N_2}}(T_{\mathrm{vib}})}{\tau_{\mathrm{N_2-e}}} \tag{24}$$

The relaxation time $\tau_{\mathrm{N_2-e}}$ is expressed as a function of electron temperature and electron pressure. It is given by the work of Lee.[14,15]

Energy loss due to dissociation and ionization

Previous researches have pointed out that a dissociation process reduces the vibrational energy content by an amount much greater than the average vibrational energy.[10] This is because a dissociation reaction causes preferably from higher vibrational energy levels in nature. Hence we have to estimate the vibrational energy removal due to dissociation with considering this effect. Such a model is referred to as the preferential dissociation model. In the present study, we assume that 50% of dissociation energy is reduced through dissociation.

$$Q_{\mathrm{D}} = \sum_{s=\mathrm{M}} \widetilde{E}_{\mathrm{D},s} \dot{w}_s^{\mathrm{D}} \tag{25}$$

$$\widetilde{E}_{\mathrm{D},s} = \frac{1}{2} E_{\mathrm{D},s} \tag{26}$$

where $\dot{w}_s^{\mathrm{D}}$ indicates the mass production rate per unit volume of species s due to dissociation. In both electron-impact dissociation and ionization, dissociation or ionization energy is given by electron translational energy, so that the loss of the electron energy due to these reactions may be written as

$$Q_{\mathrm{D}}^{\mathrm{e}} = E_{\mathrm{D,N_2}} \dot{w}_{\mathrm{N_2}}^{\mathrm{e}} \tag{27}$$

$$Q_{\mathrm{I}}^{\mathrm{e}} = E_{\mathrm{I,N}} \dot{w}_{\mathrm{N}}^{\mathrm{e}} \tag{28}$$

where $w_{\mathrm{N_2}}^{\mathrm{e}}$ and $w_{\mathrm{N}}^{\mathrm{e}}$ are mass production rate of N_2 and N due to electron impact dissociation and ionization, respectively.

4.3 Transport properties

In the present study, the coefficient of mixture viscosity, thermal conductivity and species diffusivities are evaluated by extending Yos's formula, which is based on the first Chapmann-Enskog approximation, to the multi-temperature gas mixture.[16] As for the diffusion, only mass diffusion is considered and thermal and pressure diffusion are neglected. The ambipolar diffusion is also assumed for charged species. Electrical conductivity is calculated by using the following formula:[13]

$$\tilde{\sigma} = \frac{n_e e^2}{m_e \sum_{s \neq e} \nu_{e,s}} \tag{29}$$

and Eqs. (21) and (22) are used to evaluate the collision frequency $\nu_{e,s}$.

5. Solution Method

5.1 Integration scheme

Governing equations of fluid are transformed into the generalized coordinate system and solved numerically using finite difference method. The Harten-Yee's non-MUSCL type upwind TVD scheme in a finite volume formulation[17] is employed to evaluate the numerical flux of the convective terms. The viscous, conductive and diffusive terms are simply evaluated using central difference from the application of the Gauss theorem.

In fact, many difficulties exist for the calculation of arcjet thruster including chemical or thermal nonequilibrium effects. These are mainly due to strong nonlinearity of the chemical source terms which appear in species conservation equations and of the thermal source terms in vibrational and electron energy equation. To add to them, the authors have found that thermal conduction terms are primarily responsible for the stability of electron energy equation (for highly ionized plasma flow, the electron thermal conductivity scales as $T_e^{5/2}$). In order to overcome such a difficulty, following strategies are introduced in the present calculation:

1. Point implicit procedure[18] are employed for chemical and thermal source terms of species conservation equations and vibrational energy equation.
2. Electron energy equation is treated separately from the other conservation equations, and solved iteratively with respect to the electron temperature for each time step. This is basically the same idea of Ref. 19, where steady form of the equation was employed, although in the present study the unsteady form is employed.

The equation of the electric field is also discretized in the finite difference form and solved iteratively using the SLOR (Successive Line Overrelaxation) method for each time step of the flow field integration.

The computations are performed with a hybrid scheme that consists of following sequence of operation:

1) Electrical conductivities are determined based on known temperatures and electron number densities.

2) Based on known electrical conductivities, the solutions of the electric field are obtained and Joule heating is evaluated at each grid points.

3) Electron energy equation is solved iteratively with respect to the electron temperature using the other fixed flow properties and Joule heating.

4) A set of the other propellant gas flow equations are solved based on known Joule heating and electron temperature distributions. At each time step, the time increment is determined so as to satisfy both the CFL and stability conditions to solve equations including nonlinear source terms.

5) Steps 1) to 4) are repeated until steady state solutions are attained as asymptotic solutions of the unsteady equations for large time steps.

5.2 Boundary conditions

At the inlet, the flow is assumed to be subsonic and hence it is impossible to specify all variables. Therefore, the propellant mass flow rate, temperature and degree of ionization are specified, and pressure at the inlet is determined by the zeroth extrapolation from the value at the adjacent downstream grid point. On the nozzle axis, symmetry conditions are employed. On the exit plane of the nozzle, all properties are obtained from the zeroth extrapolations. For electrode walls, non-slip conditions are imposed for each velocity components and other variables are simply extrapolated from the inner grid point. Hence detailed physical aspects of electrode wall are neglected in the present calculation.

As for the boundary conditions on the electric field, no electric currents are allowed to pass through the inlet of the thruster and the nozzle exit plane. Both anode and cathode are assumed to be equi-potential, so that

$$\phi = \begin{cases} V & \text{(on the anode surface)} \\ 0 & \text{(on the cathode surface)} \end{cases}$$

and V can be counted from the specified input power or total current. The symmetry conditions are employed on the axis of the thruster.

5.3 Initial conditions

To start the calculation with discharge, flow field with arc-off conditions (no Joule heating) are solved firstly, and ionization ratio of $\alpha = 10^{-3}$ are imposed between the cathode tip and upstream point of the constrictor thereafter without changing other primitive variables. Vibrational temperature and electron temperature are set to be equal to the translational temperature.

6. Results and Discussion

As a preliminary calculation, an operation with considerably low power was chosen in the present study. Total current was set to 1 A, and temperature and mass flow rate at the inlet were set to 300 K and 0.1 g/s, respectively.

Computational grids are shown in Fig. 2. The

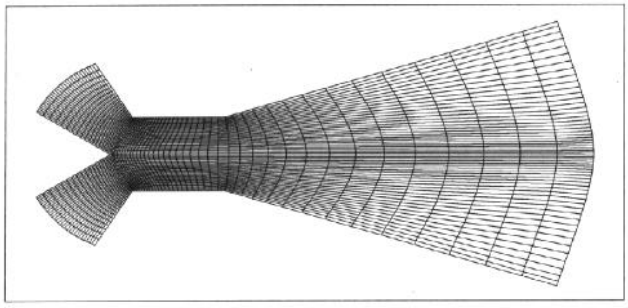

Figure 2. Computational grid

computational domain was set from 2 mm upstream of the cathode tip to 10 mm downstream of the constrictor exit. Grids were set to 58 and 30 points in the axial direction and radial direction, respectively. The grid system was generated by solving an elliptic partial differential equation with adding source terms which control orthogonality and minimum grid spacing at the boundary.

Figure 3 shows translational temperature contours. The maximum is just downstream the cathode tip. It has been found that the initial setting of the degree of ionization in upstream region is extremely important to obtain proper solutions. If it is somewhat larger, the arc attaches more upstream part of the constrictor. With adding this fact, at the initial stage of the calculation, diffusion can cause upstream attachment

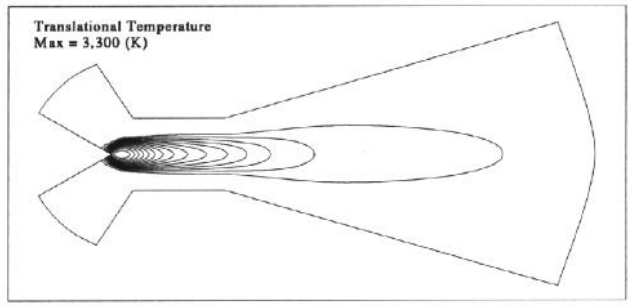

Figure 3. Translational temperature contours

of the arc column and numerical instability. This may be due to overestimation of the diffusion speed which is caused by steep local gradients of the variables. In this calculation, the flow field without diffusion was solved firstly, and it was included thereafter. The trend of vibrational temperature and electron temperature profiles are almost same as that of translational temperature, although they are not shown here.

Mole fraction contours of electron are shown in Fig. 4. The maximum degree of ionization is 1.3×10^{-3}

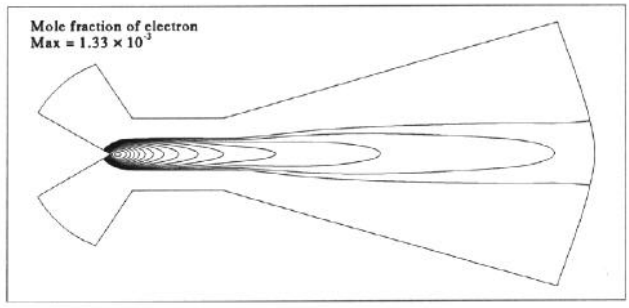

Figure 4. Mole fraction contours of electron (logarithmic scale)

just downstream the cathode tip.

Axial distributions of the three temperatures along the centerline are compared in Fig. 5. In contrast to the initial guess, the differences between each temperatures are considerably large. The electron temperature departs from other temperatures seriously ($T_e \approx 40{,}000$ K at the cathode tip). However, it decreases rapidly downstream the cathode tip and reaches equilibrium with the translational temperature in the middle of the constrictor. This result, which is in contrast to the other result of nonequilibrium nozzle flow computation[20], is probably due to overestimation of inelastic loss factor (δ, which has been discussed in Sec. 4.2) in this region. On the other hand, the vibrational temperature does not decrease so rapidly and considerably departs from other temperatures at the nozzle exit. This is because both

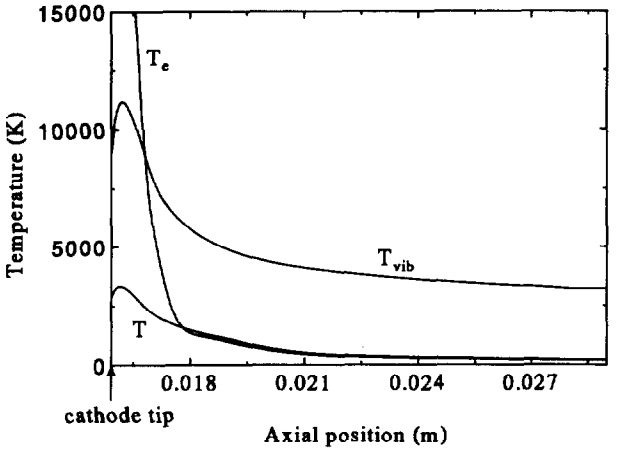

Figure 5. Axial profiles of temperature

the collision frequency and relaxation time are described by T and T_e in the present model, so that the vibrational temperature can not be relaxed in the nozzle part where T and T_e decreases rapidly, although the differences between each temperatures are relatively large.

In fact, appropriate estimation of the inelastic loss factor remains one of the most urgently needed future tasks for the calculation of arcjet thruster assuming thermal nonequilibrium, as pointed out by other works.[1,8] The electron temperature may be raised mainly by translation-electron energy exchanges because the translation-vibration relaxation time is described only by translational temperature (that is, translation-vibration energy exchange can hardly occur for $T < 3,000$ K). As for three-temperature models, the authors have found that if smaller inelastic loss factor (for example, $\delta = 10$) is used, the vibrational temperature reaches equilibrium with the electron temperature more closely, however, translation-electron energy exchange process becomes so inefficient that the translational temperature is hardly heated enough to dissociate the molecular nitrogen.

The contribution of the internal energy mode (vibrational temperature in this case) to the chemical reaction rates is also extremely important. In this study, Park's effective temperature model has been used in order to account the vibrational nonequilibrium effect as discussed in Sec. 4.1, so that the reaction rate coefficients are evaluated by a geometric average between T and T_{vib}. In this case the chemical reaction rates are strongly sensitive to the thermal nonequilibrium state, since the chemical reaction rates are exponential functions of temperature. However it is quite doubtful whether such a empirical model can be applied to arcjet thruster flows directly. This is because such a model has been constructed using the experimental data behind shock wave, where the energy exchange process is apparently different from that of arcjet thruster flow (behind the strong shock wave the energy is transferred from the translational-rotational energy to vibrational or electron energy, whereas from electron to vibrational or translational-rotational for the arcjet thruster flow). The application of such a model to the arcjet thruster flow corresponds to the implication of the reversible nature of each energy exchange processes. This problem is still unclear.

7. Summary and future works

The internal flow in an arcjet thruster with nitrogen as a working gas has been modeled using three-temperature kinetic model and analyzed numerically by using finite difference method. Considerably severe thermal nonequilibrium has been observed. As the future work, we plan to extend the present calculation to 1 kw class arcjet thruster with considering more detailed treatment of electrode boundary conditions including sheath effects. Furthermore the result is to be compared with the existing experimental data to examine the versatility of the present kinetic models.

References

[1] Martinez-Sanchez, M. and Miller, S.A., "Arcjet Modeling: Status and Prospects," *J. Propulsion and Power*, Vol.12, No.6, 1996, pp. 1035–1043.

[2] Nishida, M., Kaita, K. and Tanaka, K.: Numerical Study of the Flow Field in a DC Arcjet Thruster, Proc. 20th Int. Electric Propulsion Conf., Garmisch-Partenkirchen, Germany, pp. 591–597 (1988).

[3] Tanaka, K., Tsuchiya, K., Kaita, K. and Nishida, M.: Computational Investigation on the Characteristics of a Low Power DC Arcjet Thruster, Proc. 20th Int. Electric Propulsion Conf., Garmisch-Partenkirchen, Germany, pp. 598–605 (1988).

[4] Okamoto, H., Nishida, M. and Tanaka, K.: Numerical Studies of the Flow Field in a Low Power DC Arcjet Thruster Using Navier–Stokes Equations, Proc. 22nd Int. Electric Propulsion Conf., Viareggio, Italy, Paper 91–112 (1991).

[5] Okamoto, H., Nishida, M. Tanaka, K. and Beylich, A: Numerical Simulation of the Performance of a Radiation-cooled 1 kw DC Arcjet Thruster, Proc.

23rd Int. Electric Propulsion Conf., Seattle, U.S.A., pp. 1655–1661 (1993).

[6] Okamoto, H., Nishida, M., Tanaka, K. and Beylich, A., "Numerical Studies of an Arc-Heated Nozzle Flow for a Low Power Arcjet Thruster," *Computational Fluid Dynamics JOURNAL*, Vol. 4, No. 2, 1995, pp. 177–190.

[7] Fujita, K. and Arakawa, Y.: Numerical Prediction of Arcjet Performance Based on the Chemical Kinetics and Electron Temperature Disparity, Proc. 24th Int. Electric Propulsion Conf., Moscow, pp. 183–192 (1995).

[8] Megli, T.W., Krier, H., Burton, R.L. and Mertogul, A., "Two-Temperature Plasma Modeling of Nitrogen/Hydrogen Arcjets," *Journal of Propulsion and Power*, Vol. 12, No. 6, 1996, pp. 1062–1069.

[9] Miller, S.A. and Martinez-Sanchez, M., "Two-Fluid Nonequilibrium Simulation of Hydrogen Arcjet Thrusters," J. Propulsion and Power, Vol. 12, 1996, pp. 112–119.

[10] Park, C., *Nonequilibrium Hypersonic Aerothermodynamics*, Wiley, New York, 1990.

[11] Millikan, R.C. and White, D.R., "Systematics of Vibrational Relaxation," *J. Chem. Phys.*, Vol. 39, 1963, pp. 3209–3213.

[12] Gnoffo, P.A., Gupta, R.N. and Shin, J.L., "Conservation Equations and Physical Models for Hypersonic Air Flows," NASA TP-2867, 1989.

[13] Mitchner, M. and Kruger, Jr., C. H., *Partially Ionized Gases*, Wiley, New York, 1973.

[14] Lee, J.-H., "Electron-Impact Vibrational Excitation Rates in the Flowfield of Aeroassisted Orbital Transfer Vehicles," *Thermophysical Aspects of Reentry Flows*, Vol. 103, Progress in Astronautics and Aeronautics, (Moss, J. N. and Scott, C. D. eds., AIAA, New York), 1985, pp. 197-224.

[15] Lee, J.-H., "Electron-Impact Vibrational Relaxation in High-Temperature Nitrogen," *J. Thermophys. Heat Trans.* , Vol. 7, No. 3, July-Sept. 1993.

[16] Gupta, R. N., Yos, J. M., Thompson, R. A., and Lee, K.-P., "A Review of Reaction Rates and Thermodynamic and Transport Properties for an 11-Species Air Model for Chemical and Thermal Nonequilibrium Calculations to 30000K," NASA RP 1232, Aug. 1990.

[17] Yee, H. C., "A Class of High-Resolution Explicit and Implicit Shock-Capturing Methods," NASA TM-101088, Feb. 1989.

[18] Bussing, T. R. A. and Murman, E. M., "A Finite Volume Method for the Calculation of Compressible Chemically Reacting Flows," AIAA-85-331, Jan. 1985.

[19] Fasoulas, S., Auweter-Kurtz, M., Habiger, H. A., Laure, S. H., and Sleziona, P. C., "Investigation of a Nitrogen Flow within a Plasma Wind Tunnel," AIAA-93-2817, July 1993.

[20] Park, C., "Validation of Multitemperature Nozzle Flow Code," *J. Thermophys. Heat Trans.* , Vol. 9, No. 1, Jan.-March, 1995.